Supplementary material

The supporting information provides additional figures with respect to the nutrient limitation of phytoplankton growth in ROMS-BEC (S1), the data coverage in a SO satellite derived chlorophyll product (S2), the model evaluation (S3-S6), the bloom timing (S7), the ecological niche analysis (S8), and the sensitivity simulations allowing for a half-saturation constant of iron of *Phaeocystis* that varies with the surrounding light levels (S9).

S1: Additional figures

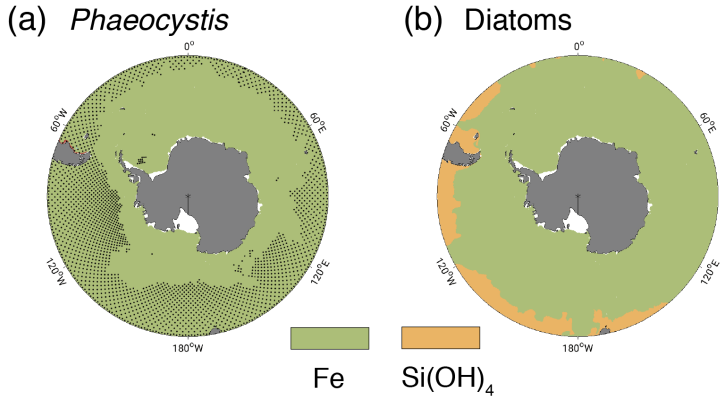

Figure S1: Annual mean most limiting nutrient at the surface south of 45° S for growth rates of a) *Phaeocystis* and b) diatoms in the *Baseline* simulation of ROMS-BEC. High-latitude phytoplankton growth in the model is most limited by either iron (green) or silicic acid (yellow, diatoms only). The stippling in panel a) denotes areas where peak monthly mean chlorophyll concentrations of Phaeocystis do not exceed 0.1 mg chl m^{-3}.

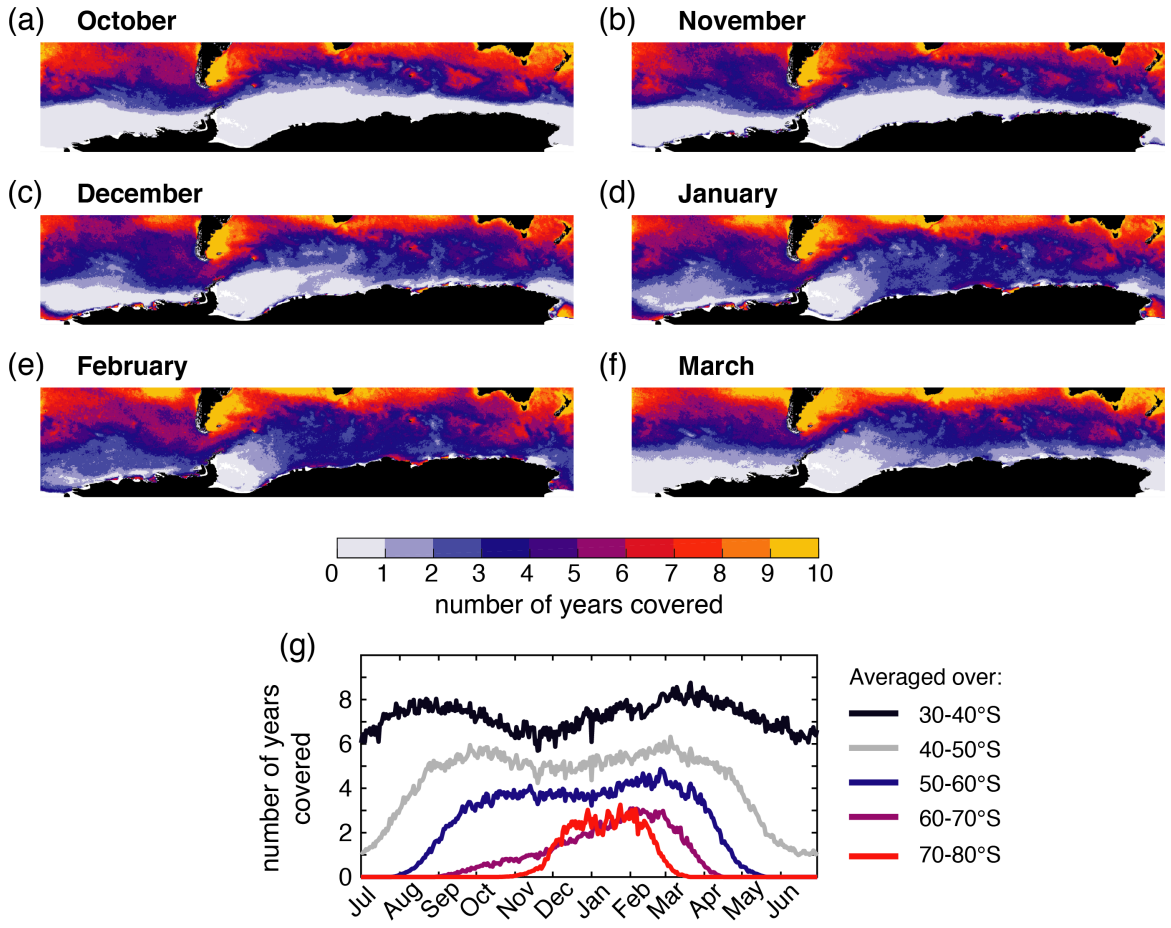

Figure S2: Assessment of the SO data coverage in the climatological (1998-2018, i.e. 21 years) daily Globcolor chlorophyll product (Fanton d'Andon et al., 2009; Maritorena et al., 2010): a)-f) Average number of years available for the calculation of the climatological chlorophyll concentration at each grid cell for each of the shown months (October-March), respectively. No minimum number of "days with data coverage" is required for a given month to be counted as "data available" (i.e. one day of data coverage in a month is enough for that month to be counted as "covered" in the respective year). g) Average number of years available for the calculation of the climatological chlorophyll concentration on each day for 10° latitudinal bands across the SO.

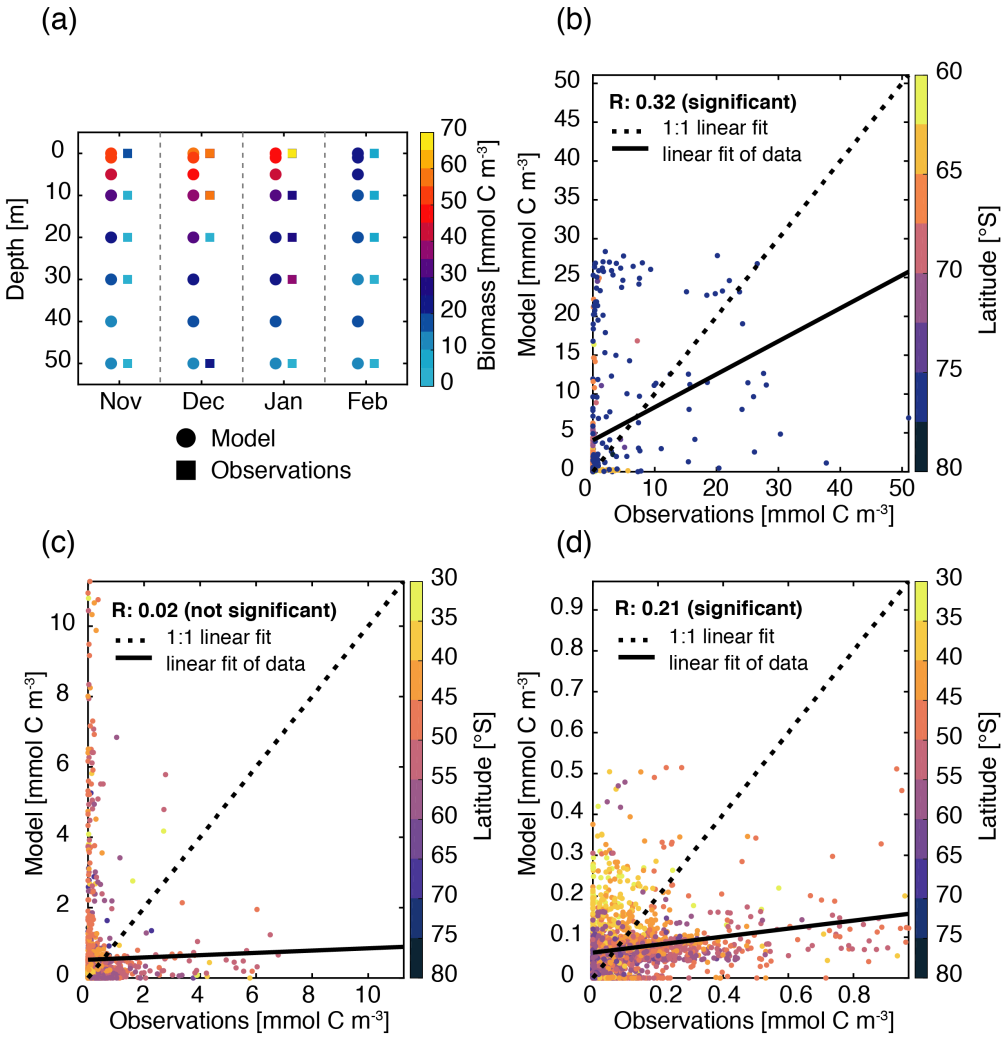

Figure S3: Validation of a) & b) *Phaeocystis*, c) diatom, and d) coccolithophore carbon biomass [mmol C m^{-3}]. Panel a) shows the maximum *Phaeocystis* carbon biomass concentrations [mmol C m^{-3}] in ROMS-BEC (circles) and in observations (squares, Vogt et al., 2012) for each month between November-February and in the the upper 50 meters of the water column. For panels b)-d), the model output is colocated with observations in space and time, and observational data from all months and from above 1000 m are considered here (Balch et al., 2016; Saavedra-Pellitero et al., 2014; O'Brien et al., 2013; Vogt et al., 2012; Leblanc et al., 2012; Tyrrell and Charalampopoulou, 2009; Gravalosa et al., 2008; Cubillos et al., 2007). For more details on the biomass evaluation, see Nissen et al. (2018). The dotted line shows the perfect linear 1:1 fit, whereas the solid line is the actual fit of the data (linear regression). Pearson correlation coefficients of these regressions are given in the top right, those for *Phaeocystis* and coccolithophores are statistically significant ($p<0.05$). Points are color-coded according to the sampling latitude.

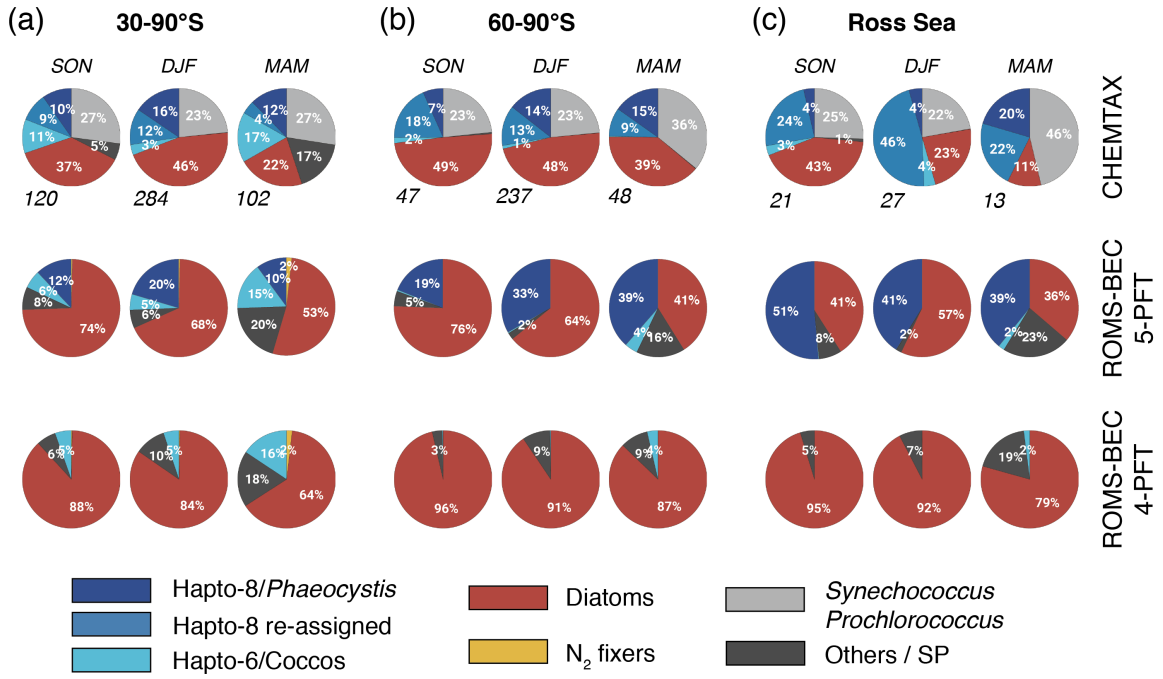

Figure S4: a)-c) Relative contribution of the five phytoplankton PFTs to total chlorophyll biomass [mg chl m^{-3}] for a) 30-90° S, b) 60-90° S, and c) the Ross Sea. The top pie charts denote the climatological mixed layer average community composition suggested by CHEMTAX analysis of HPLC pigments for spring, summer, and fall, respectively (the total number of available observations for a given region and season is given at the lower left side, Swan et al., 2016), and the lower pie charts denote the corresponding community structure in the top 50 m in ROMS-BEC in the 5-PFT setup (middle row, same as in Fig. 2 in the main text) and in the 4-PFT setup (lowest row, no *Phaeocystis*, Nissen et al., 2018), respectively. Note that the categories in the CHEMTAX analysis are not 100% equivalent to the model PFTs, and here, "Hapto-8 reassigned" corresponds to the contribution of Hapto-6 where the temperature is <2°C (see also section 2.3.1 in the main text).

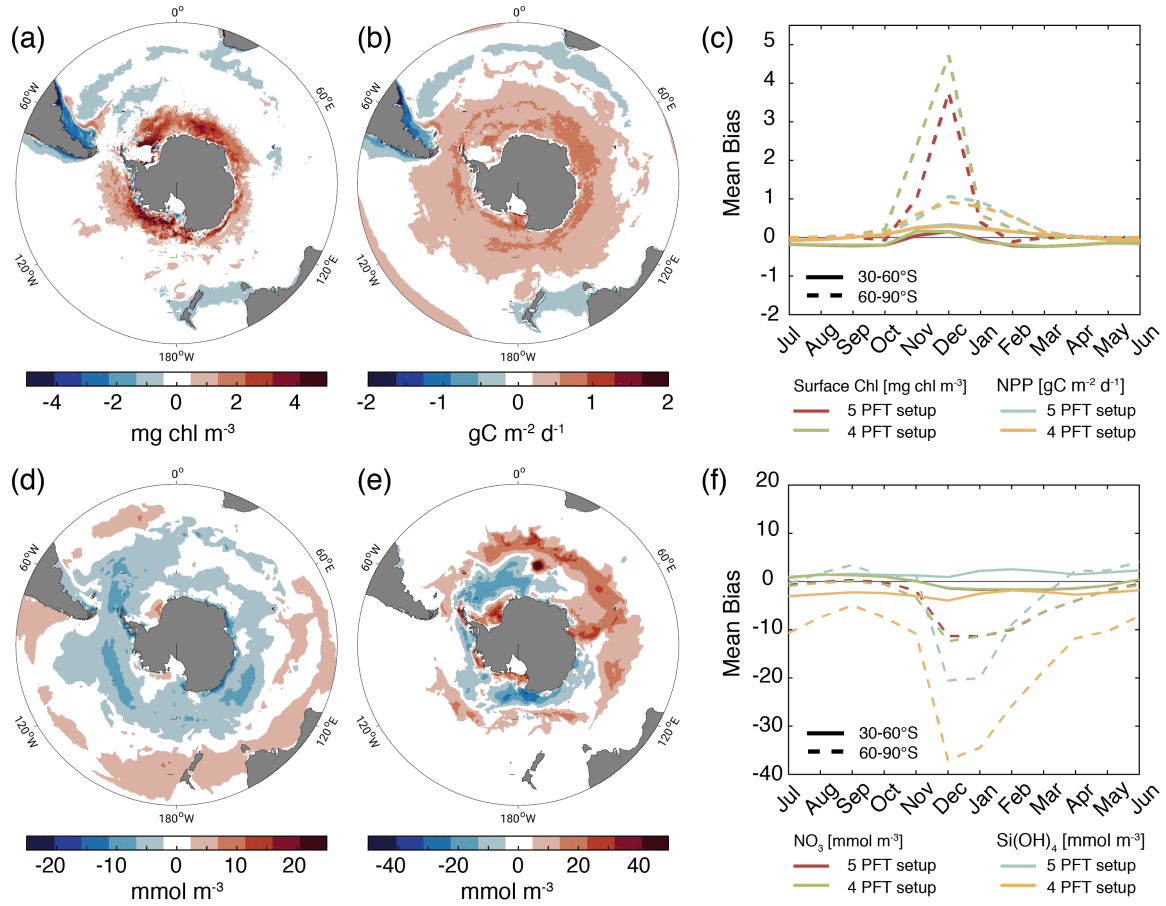

Figure S5: Annual mean bias (*Baseline* simulation minus observations) of a) total surface chlorophyll concentrations [g chl m^{-3}], b) total vertically integrated NPP [mg C m^{-2} d^{-1}], d) surface nitrate concentrations [mmol m^{-3}], and e) surface silicic acid concentrations [mmol m^{-3}]. The panels c) & f) denote the temporal evolution of the model bias of c) total surface chlorophyll concentration (red) and total NPP (blue), as well as f) surface nitrate concentrations (red), and silicic acid concentrations (blue) in the 5-PFT setup of ROMS-BEC between 30-60° S (solid) and 60-90° S (dashed), respectively. For comparison, the model bias obtained with the 4 PFT setup of ROMS-BEC is included in both panels in green (chlorophyll and nitrate) and yellow (NPP and silicic acid), respectively (see also supplement in Nissen et al., 2018).

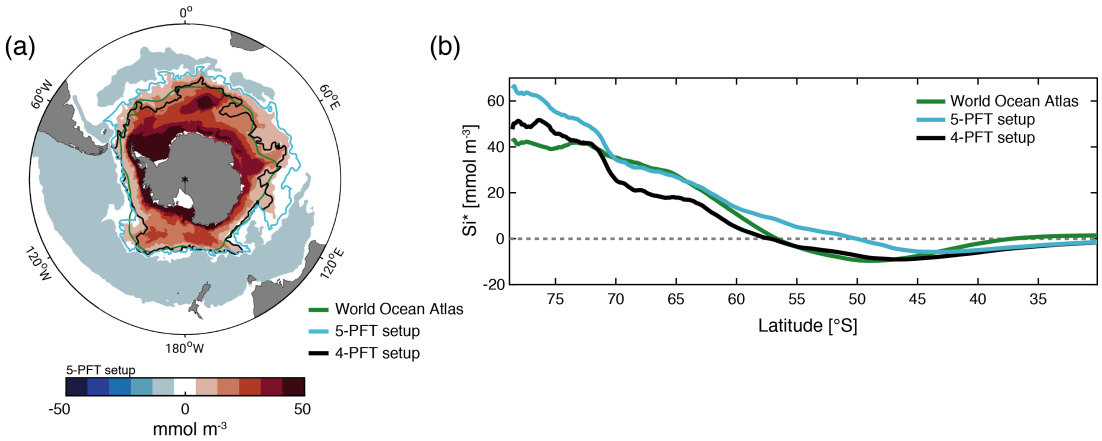

Figure S6: Annual mean top 100 m average a) Si* [mmol m^{-3}], which is defined as the difference in concentration between silicic acid and nitrate (Freeman et al., 2018), in the *Baseline* simulation of the 5-PFT setup of ROMS-BEC (colors). The contours denote the latitude of the silicate front, i.e. where Si*=0, in data from the World Ocean Atlas (green, Garcia et al., 2014) and in the *Baseline* simulation of the 5-PFT setup (light blue) and the 4-PFT setup (black, Nissen et al., 2018) of ROMS-BEC, respectively. b) zonal average Si* [mmol m^{-3}], colors are the same as the contours in panel a).

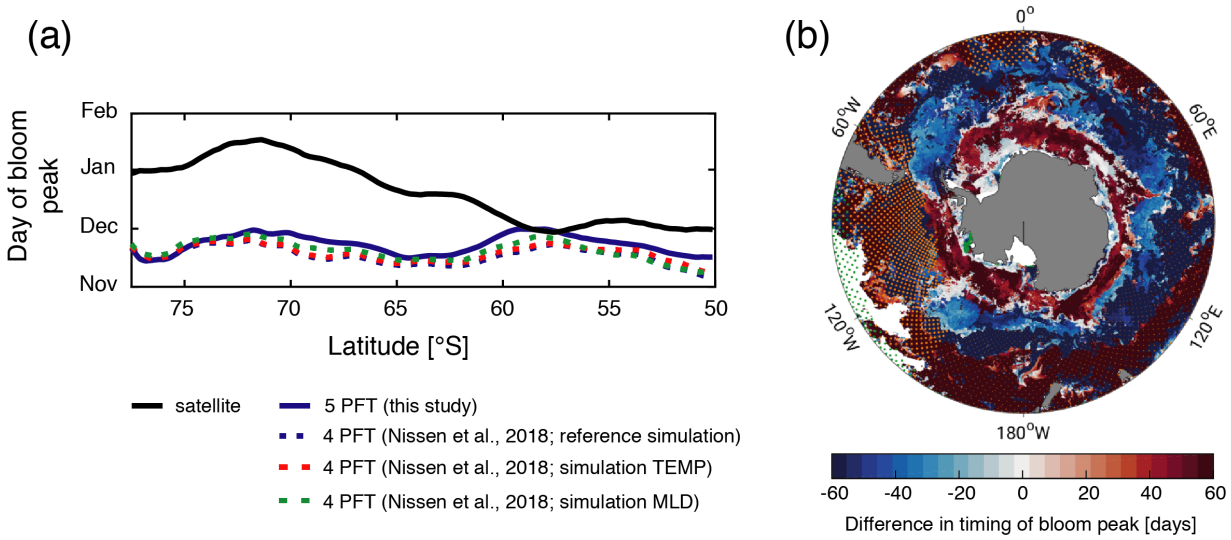

Figure S7: a) Same as Fig. 3 in the main text, Hovmoller plots south of 50° S of the day of maximum total chlorophyll concentrations in a satellite product (black line, Globcolor climatology from 1998-2018 based on the daily 25 km chlorophyll product, see Fanton d'Andon et al., 2009; Maritorena et al., 2010), the *Baseline* simulation of this study (solid blue line), the *Baseline* simulation of Nissen et al. (2018, dashed blue line; without *Phaeocystis*). Additionally, two sensitivity simulations in the 4 PFT setup from Nissen et al. (2018) are shown here to show the impact of biases in the simulated physical fields on phytoplankton phenology: The simulations TEMP (dashed red line) and MLD (dashed green line) correct for the simulated average temperature and MLD biases, respectively, within the biological subroutine of the model. b) Difference in day of bloom peak between *Phaeocystis* and diatoms, based on chlorophyll concentrations in the 5-PFT *Baseline* simulation. Stippling indicates locations where maximum chlorophyll concentrations never exceed 0.1 mg chl m^{-3} for *Phaeocystis* (orange) and diatoms (green), respectively. White areas correspond to areas where the peak total chlorophyll concentrations do not exceed 0.5 mg chl m^{-3}.

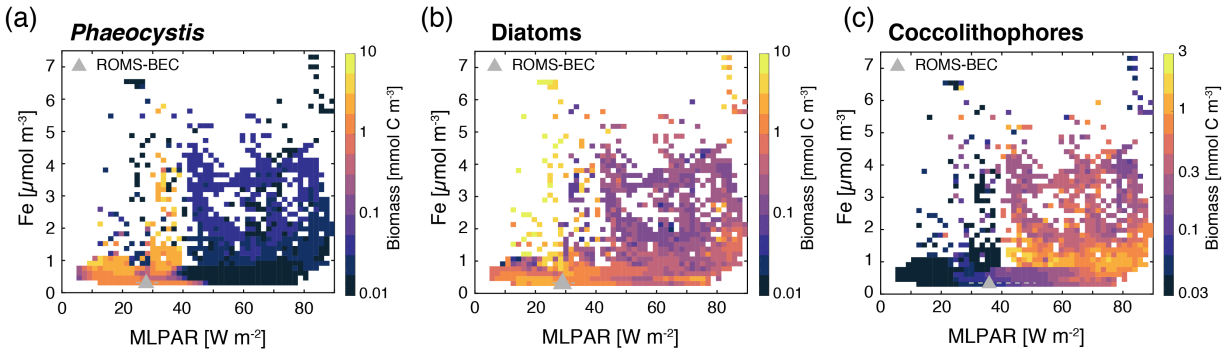

Figure S8: Simulated DJFM average top 50 m average a) *Phaeocystis*, b) diatom, and c) coccolithophore carbon biomass concentrations [mmol C m^{-3}] south of 40° S as a function of the simulated concurrent dissolved iron concentrations [μmol Fe m^{-3}] and mixed layer PAR levels (W m^{-2}) in the 5-PFT *Baseline* simulation of ROMS-BEC. Overlain are the simulated area and biomass weighted ecological niche centers (median, triangle) and breadths (inter quartile ranges, dashed lines) for the three functional types.

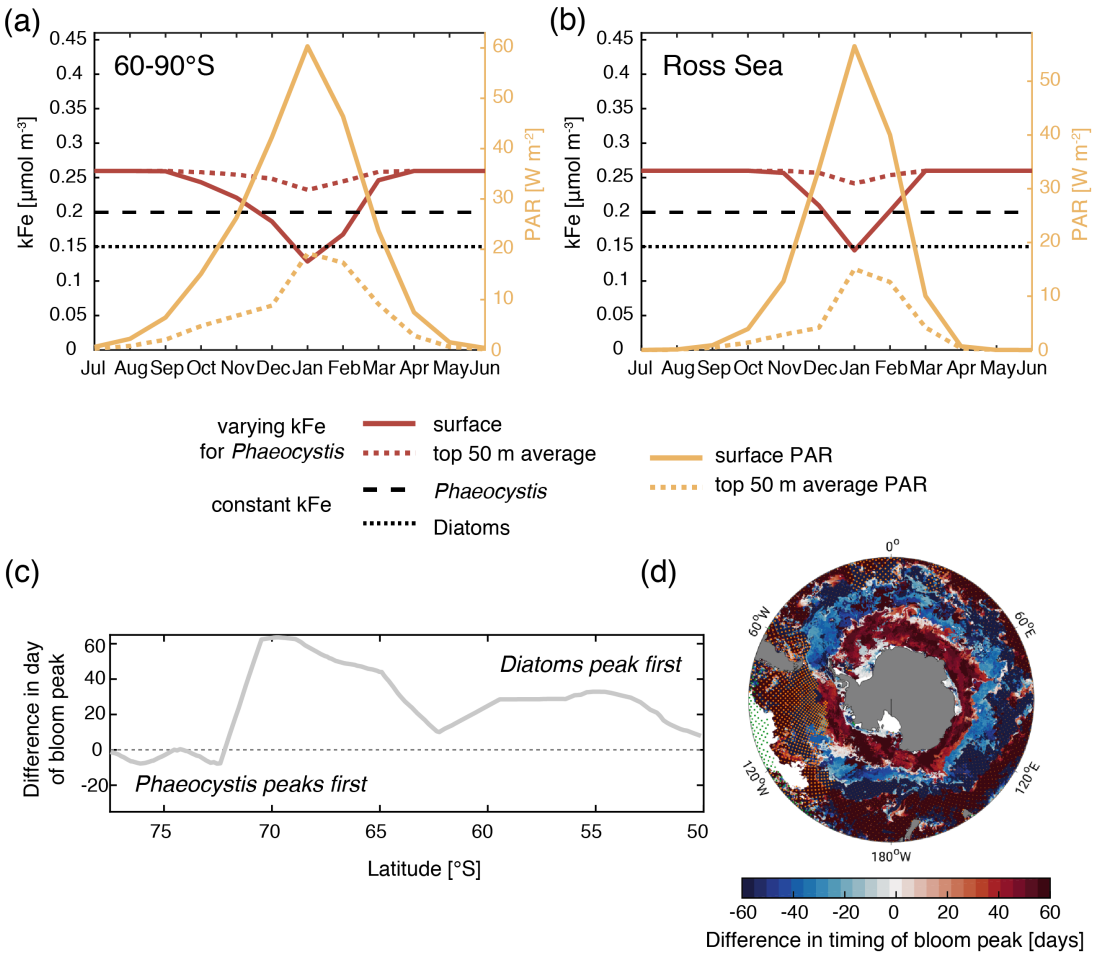

Figure S9: Results from the simulation VARYING_kFE (see section 2.2 in the main text): Varying half-saturation constant of iron of *Phaeocystis* (k_{Fe}, red, left y axis) and PAR (yellow, right y axis) as a function of time (x axis) for the surface (solid) and averaged over the top 50 m (dashed) for a) between 60-90° S and b) in the Ross Sea. Black lines indicate the constant k_{Fe} of *Phaeocystis* (dashed) and diatoms (dotted) used in the *Baseline* simulation of this study. c) Difference in days in the timing of the bloom peak of diatoms and *Phaeocystis* for each latitude, with negative values denoting a succession from *Phaeocystis* to diatoms throughout the season. d) Difference in day of bloom peak between *Phaeocystis* and diatoms. Stippling indicates locations where maximum chlorophyll concentrations never exceed 0.1 mg chl m^{-3} for *Phaeocystis* (orange) and diatoms (green), respectively. White areas correspond to areas where the peak total chlorophyll concentrations do not exceed 0.5 mg chl m^{-3}.

References

Balch, W. M., Bates, N. R., Lam, P. J., Twining, B. S., Rosengard, S. Z., Bowler, B. C., Drapeau, D. T., Garley, R., Lubelczyk, L. C., Mitchell, C., and Rauschenberg, S.: Factors regulating the Great Calcite Belt in the Southern Ocean and its biogeochemical significance, Global Biogeochemical Cycles, 30, 1199–1214, https://doi.org/10.1002/2016GB005414, 2016.

Cubillos, J. C., Wright, S. W., Nash, G., de Salas, M. F., Griffiths, B., Tilbrook, B., Poisson, A., and Hallegraeff, G. M.: Calcification morphotypes of the coccolithophorid *Emiliania huxleyi* in the Southern Ocean: changes in 2001 to 2006 compared to historical data, Marine Ecology Progress Series, 348, 47–54, https://doi.org/10.3354/meps07058, 2007.

Fanton d'Andon, O., Mangin, A., Lavender, S., Antoine, D., Maritorena, S., Morel, A., Barrot, G., Demaria, J., and Pinnock, S.: GlobColour - the European Service for Ocean Colour, in: Proceedings of the 2009 IEEE International Geoscience & Remote Sensing Symposium, IEEE International Geoscience & Remote Sensing Symposium (IGARSS), ISBN: 9781424433957, 2009.

Freeman, N. M., Lovenduski, N. S., Munro, D. R., Krumhardt, K. M., Lindsay, K., Long, M. C., and Maclennan, M.: The variable and changing Southern Ocean silicate front: Insights from the CESM large ensemble, Global Biogeochemical Cycles, 32, 752–768, https://doi.org/10.1029/2017GB005816, 2018.

Garcia, H. E., Locarnini, R. A., Boyer, T. P., Antonov, J. I., Baranova, O. K., Zweng, M. M., Reagan, J. R., and Johnson, D. R.: World Ocean Atlas 2013, Volume 4 : Dissolved inorganic nutrients (phosphate, nitrate, silicate), NOAA Atlas NESDIS 76, 4, 25 pp, 2014.

Gravalosa, J. M., Flores, J.-A., Sierro, F. J., and Gersonde, R.: Sea surface distribution of coccolithophores in the eastern Pacific sector of the Southern Ocean (Bellingshausen and Amundsen Seas) during the late austral summer of 2001, Marine Micropaleontology, 69, 16–25, https://doi.org/10.1016/j.marmicro.2007.11.006, 2008.

Leblanc, K., Arístegui, J., Armand, L., Assmy, P., Beker, B., Bode, A., Breton, E., Cornet, V., Gibson, J., Gosselin, M.-P., Kopczynska, E., Marshall, H., Peloquin, J., Piontkovski, S., Poulton, A. J., Quéguiner, B., Schiebel, R., Shipe, R., Stefels, J., van Leeuwe, M. A., Varela, M., Widdicombe, C., and Yallop, M.: A global diatom database - abundance, biovolume and biomass in the world ocean, Earth System Science Data, 4, 149–165, https://doi.org/10.5194/essd-4-149-2012, 2012.

Maritorena, S., Fanton D'Andon, O., Mangin, A., and Siegel, D. A.: Merged satellite ocean color data products using a bio-optical model: Characteristics, benefits and issues, Remote Sensing of Environment, 114, 1791–1804, https://doi.org/10.1016/j.rse.2010.04.002, 2010.

Nissen, C., Vogt, M., Münnich, M., Gruber, N., and Haumann, F. A.: Factors controlling coccolithophore biogeography in the Southern Ocean, Biogeosciences, 15, 6997–7024, https://doi.org/10.5194/bg-15-6997-2018, 2018.

O'Brien, C. J., Peloquin, J. A., Vogt, M., Heinle, M., Gruber, N., Ajani, P., Andruleit, H., Arístegui, J., Beaufort, L., Estrada, M., Karentz, D., Kopczyńska, E., Lee, R., Poulton, A. J., Pritchard, T., and Widdicombe, C.: Global marine plankton functional type biomass distributions: coccolithophores, Earth System Science Data, 5, 259–276, https://doi.org/10.5194/essd-5-259-2013, 2013.

Saavedra-Pellitero, M., Baumann, K.-H., Flores, J.-A., and Gersonde, R.: Biogeographic distribution of living coccolithophores in the Pacific sector of the Southern Ocean, Marine Micropaleontology, 109, 1–20, https://doi.org/10.1016/j.marmicro.2014.03.003, 2014.

Swan, C. M., Vogt, M., Gruber, N., and Laufkötter, C.: A global seasonal surface ocean climatology of phytoplankton types based on CHEMTAX analysis of HPLC pigments, Deep-Sea Research Part I, 109, 137–156, https://doi.org/10.1016/j.dsr.2015.12.002, 2016.

Tyrrell, T. and Charalampopoulou, A.: Coccolithophore size, abundance and calcification across Drake Passage (Southern Ocean), 2009, https://doi.org/10.1594/PANGAEA.771715, 2009.

Vogt, M., O'Brien, C., Peloquin, J., Schoemann, V., Breton, E., Estrada, M., Gibson, J., Karentz, D., Van Leeuwe, M. A., Stefels, J., Widdicombe, C., and Peperzak, L.: Global marine plankton functional type biomass distributions: *Phaeocystis* spp., Earth System Science Data, 4, 107–120, https://doi.org/10.5194/essd-4-107-2012, 2012.